Interplay between ShcA signaling and PGC-1α triggers targetable metabolic vulnerabilities in breast cancer

*Young Kyuen Im[1,2], *Ouafa Najyb[3,5], Simon-Pierre Gravel[3,5], Shawn McGuirk[3,5], Ryuhjin Ahn[1,2], Daina Z. Avizonis[5], Valérie Chénard[3,5], Valerie Sabourin[1], Jesse Hudson[1,2], Tony Pawson[6], Ivan Topisirovic[1,2,3,4], Michael Pollak[1,2,4], Julie St-Pierre[3,5,7]** and Josie Ursini-Siegel[1,2,3,4]**

*YKI and ON contributed equally to this work **JUS and JSP are co-senior authors

[1]Lady Davis Institute for Medical Research, 3755 Chemin de la Côte-Sainte-Catherine, Montréal, QC, Canada. H3T 1E2; [2]Division of Experimental Medicine, McGill University, 1001 Decarie Boulevard, H4A 3J1; [3]Department of Biochemistry, McIntyre Medical Building, McGill University, 3655 Promenade Sir William Osler, H3G 1Y6; [4]Gerald Bronfman Department of Oncology, McGill University 5100 Maisonneuve Blvd West, McGill University, H4A 3T2; [5]Goodman Cancer Research Centre, 1160 Avenue des Pins, Montréal, QC, Canada. H3A 1A3; [6]The Lunenfeld-Tanenbaum Research Institute, Sinai Health System, 600 University Ave., Toronto, ON, Canada. M5G 1X5; [7]Departments of Biochemistry, Microbiology and Immunology and Ottawa Institute of Systems Biology, University of Ottawa, 451 Smyth Road, K1H 8M5

Running Title: ShcA signaling controls breast tumor metabolism

Conflicts: The authors declare that they have no conflict of interest.

Keywords: ShcA, PGC-1α, breast cancer, glucose, glutamine, tumor metabolism, metabolic flexibility, biguanide

Financial Support: This work was supported by CIHR grants to J. Ursini-Siegel (MOP-111143) and J. Ursini-Siegel and J. St-Pierre (MOP-244105).

**Co-corresponding Authors:

Julie St-Pierre
Ottawa Institute of Systems Biology
451 Smyth Road
Ottawa, ON, Canada, K1H 8M5

Josie Ursini-Siegel
Lady Davis Institute for Medical Research
3755 Cote St. Catherine Road
Montreal, QC, Canada, H3T 1E2

ABSTRACT

The ShcA adaptor protein transduces oncogenic signals downstream of receptor tyrosine kinases. We show here that breast tumors engage the ShcA pathway to increase their metabolism. ShcA signaling enhanced glucose catabolism through glycolysis and oxidative phosphorylation, rendering breast cancer cells critically dependent on glucose. ShcA signaling simultaneously increased the metabolic rate and flexibility of breast cancer cells by inducing the PGC-1α transcription factor, a central regulator of mitochondrial metabolism. Breast tumors that engaged ShcA signaling were critically dependent on PGC-1α to support their increased metabolic rate. PGC-1α deletion drastically delayed breast tumor onset in an orthotopic mouse model, highlighting a key role for PGC-1α in tumor initiation. Conversely, reduced ShcA signaling impaired both the metabolic rate and flexibility of breast cancer cells, rendering them reliant on mitochondrial oxidative phosphorylation. This metabolic reprogramming exposed a targetable metabolic vulnerability, leading to a sensitization of breast tumors to inhibitors of mitochondrial complex I (biguanides). Genetic inhibition of ShcA signaling in the Polyoma virus middle T (MT) breast cancer mouse model sensitized mammary tumors to biguanides during the earliest stages of breast cancer progression. Tumor initiation and growth were selectively and severely impaired in MT/ShcA-deficient animals. These data demonstrate that metabolic reprogramming is a key component of ShcA signaling and serves an unappreciated yet vital role during breast cancer initiation and progression. These data further unravel a novel interplay between ShcA and PGC-1α in the coordination of metabolic reprogramming and demonstrate the sensitivity of breast tumors to drugs targeting oxidative phosphorylation.

Significance: This study uncovers a previously unrecognized mechanism that links aberrant RTK signaling with metabolic perturbations in breast cancer and exposes metabolic vulnerabilities that can be targeted by inhibitors of oxidative phosphorylation.

INTRODUCTION

Metabolic reprogramming represents an emerging hallmark in order for cancers to meet their energetic and biosynthetic demands (1). To achieve this, cancer cells coordinate ATP-producing (glycolysis and oxidative phosphorylation) and ATP-consuming (protein, nucleotide and lipid synthesis) processes. This reprogramming is often coupled to distinct nutrient dependencies, exposing targetable metabolic vulnerabilities that are being exploited in cancer clinical trials. For example, Warburg-like cancers undergo glycolysis, even when oxygen levels are plentiful. Pyruvate is preferentially converted to lactate instead of being fully metabolized through the citric acid cycle (CAC) and oxidative phosphorylation for further ATP generation (2). This adaptive response permits increased biosynthesis to support cell division. Warburg-like tumors compensate for inefficient ATP production by increasing glucose uptake, which forms the basis for ^{18}Fluorodeoxyglucose (FDG)-Positron Emission Tomography (PET) imaging as a diagnostic tool to detect malignant lesions (3). Indeed, a non-hydrolyzable glucose analogue (2-deoxy-D-glucose) is being tested as a therapeutic in Warburg-like cancers (4), including in combination with tyrosine kinase inhibitors (5,6).

Some aggressive cancers also use glutamine to increase ATP production and synthesis of CAC intermediates through reductive carboxylation to support lipid synthesis (7,8). This requires the activity of two glutaminases (GLS1, GLS2), which convert glutamine to glutamate. Glutamate can be used as an intermediate for amino acid synthesis, redox balance or it can enter the CAC through its conversion into α-

ketoglutarate (8). Indeed, glutaminase inhibitors exert potent anti-neoplastic effects in a subset of cancers, including triple negative breast cancers (9).

Cancers that are strictly glutamine-addicted require a functional CAC to meet their energetic demands. This is consistent with the observation that decreased glutamine flux through the CAC sensitizes tumors to the anti-neoplastic effects of metformin (10), a biguanide that is commonly used to treat type II diabetes (11). Biguanides, including metformin and phenformin, block complex I of the electron transport chain (12-14) to inhibit mitochondrial ATP production, rendering cells critically dependent on glycolysis (10,12,15). This forms the basis for increased sensitivity of tumors to glycolysis inhibitors in combination with biguanides (16).

Breast cancers are classified into distinct subtypes, including ER+, HER2+ and triple negative. Of these, HER2+ and triple negative breast cancers are associated with the worst outcome and are driven by receptor tyrosine kinase (RTK) signaling. These breast cancers display significant metabolic rewiring, including increased rates of glucose and glutamine metabolism (17). RTKs increase breast tumor growth, in part, by promoting glycolytic metabolism (18-20). The ShcA adaptor is a modular protein that transduces phospho-tyrosine (pY) dependent signals downstream of RTKs (21). Genetic studies showed that the ShcA pathway is essential for breast cancer progression (22-25).

The rapid growth of aggressive breast tumors requires the coordination of two fundamental processes. First, tumors must increase angiogenesis, to acquire the requisite oxygen and nutritional support to fuel their growth (26). Second, cancer cells must capitalize on this rise in nutrient supply with a simultaneous increase in their metabolic rate to meet the energetic demands of biosynthesis required for unrestrained cell

proliferation. Given previous observations that RTKs engage ShcA to coordinately increase breast cancer proliferation and angiogenesis (23,25), we reasoned that this pathway would also play a central role in metabolic rewiring of breast cancer cells. Indeed, we identified a novel role for ShcA in coordinating metabolic reprogramming of breast cancers. ShcA upregulates the expression and activity of the key metabolic regulator, PGC-1α, in breast cancer cells, leading to an elevated global bioenergetic capacity and increased glucose dependency. Attenuation of ShcA signaling reduces the metabolic rate of breast cancer cells and makes them more dependent on glutamine. Moreover, the anti-neoplastic effects of biguanides are potentiated when ShcA signaling is impeded in mammary tumors. Thus, the ShcA/PGC-1α axis is a novel determinant of metabolic reprogramming and sensitivity to metabolic disrupters, such as biguanides.

MATERIALS AND METHODS

Cell Lines. NMuMG-NT2197 are immortalized NMuMG mouse mammary epithelial cells that were obtained from the ATCC and subsequently transformed with an oncogenic variant of rat ErbB2 (Neu) and have been described previously (27). The stable cell lines overexpressing wild-type ShcA ($ShcA^{WT}$) or a ShcA-Y239/240/313F mutant (Shc3F) were also described (25). ErbB2/Shc3F cells were further transfected with pQCXIB/PGC1α or pQCXIB empty vector to generate (PGC1α O/E) and Shc3F (EV) respectively. To generate the PGC-1α/pQCXIB vector, PGC-1α was sub-cloned from pcDNA-f:PGC1 (Addgene Plasmid#1026). The MT/$ShcA^{+/+}$ and MT/$Shc^{3F/+}$ cell lines employed in this study were generated from MMTV/MT transgenic mouse mammary tumors and described elsewhere (25,28). Nutrient deprivation media consists of all the components of control media except for DMEM, where No Glucose DMEM (0 mM glucose; Cat#319-061-CL, Wisent), Low Glucose DMEM (5 mM glucose; Cat#319-010-CL, Wisent), or No Glutamine DMEM (0 mM glutamine; Cat#319-025-CL, Wisent) was used instead. For the nutrient starvation experiments, the media was refreshed every 2-3 days. All cell lines were not cultured for longer than one month prior to replenishing with a fresh stock of cells. Cell authentication was not performed as the NMuMG cell line used was purchased from the ATCC and the MT/ShcA cell lines were established by our group from MMTV/MT transgenic tumors. All cell lines were routinely tested for mycoplasma using the Mycoprobe mycoplasma detection kit (R&D; Cat# CUL00IB).

Mice. MMTV/MT have been described (28). Mice expressing mutant ShcA protein containing tyrosine-to-phenylalanine point mutations at residues 239/240/313 (Shc3F) under the control of the endogenous *ShcA* promoter have been described (29). SCID-

Beige mice were purchased from Charles River Laboratories. For mammary fat pad injection, 5 x 10^5 cells were injected into the fourth mammary fat pad of female mice (6 - 10 weeks of age). Tumor growth was monitored every two days via caliper measurements and tumor volumes were calculated as previously described (25). Phenformin (Cat#P296900, Toronto Research Chemicals) treatment was carried out via daily intraperitoneal injection (50 mg/kg) for the orthotopic studies. For the transgenic studies, MMTV/ShcA$^{+/+}$ and MMTV/ShcA$^{3F/+}$ transgenic mice were monitored for tumor onset by bi-weekly physical palpation and following detection of one tumor-bearing gland, were either given water alone or received 200 mg/kg phenformin in their drinking water with 50mg/ml of sucrose for 4-5 weeks, where fresh phenformin was administered 2~3 times per week. All animal studies were approved by the Animal Resources Council (ARC) at McGill University and comply with guidelines set by the Canadian Council of Animal Care.

Seahorse Respirometry. Extracellular acidification rates (ECAR) and oxygen consumption rates (OCR) were measured using an XF24 Seahorse instrument (Extracellular Flux Analyzer, Agilent, ON, Canada) per manufacturer's instructions. Briefly, cells were seeded at 30 000 cells per well in 250µL of culture media and, after incubating overnight in a 37°C incubator, cells were washed twice with XF base media (Agilent), supplemented with 25mM glucose, 4mM glutamine, and 1mM sodium pyruvate. A final volume of 525µL supplemented XF media was added, and the plate was set to incubate for 1 hour in a CO2-free incubator at 37°C. OCR and ECAR were obtained by repeated cycles of mix (3min), pause (3min), and measurement (3min). Measurements were normalized on protein content at the end of the experiment. %

glycolysis rate and % respiration rate were obtained by normalizing ECAR and OCR values, respectively, to that of ErbB2/ShcA^{WT} cells.

Metabolites extraction from cells and stable isotope tracer experiment. Cells were seeded in 6-well plates and were then treated with phenformin (0.5 mM; Sigma-Aldrich, ON, Canada) or ddH_2O (control) for 24h. For stable isotope tracer experiments, cells were pre-incubated with media containing unlabelled glucose and glutamine for 2h and the media was then changed by labelled media ([U-^{13}C]-glucose (25mM in media; Cambridge Isotope Laboratories, MA, USA; CLM-1396; D-Glucose ([U-^{13}C], 99%) or with [U-^{13}C]-glutamine (4 mM in media; Cambridge Isotope Laboratories, MA, USA; CLM-1822; L-Glutamine [U-^{13}C], 99%)). Tracing to citric acid cycle intermediates with [U-^{13}C]-glucose or [U-^{13}C]-glutamine were performed at 15, 30, 60, and 120 minutes, and DHAP, lactate, and pyruvate isotopomer analyses were performed with [U-^{13}C] glucose for 30, 60, 90 and 300 seconds to ensure measurements were in the dynamic range of labeling (30). After washing twice in cold saline solution (NaCl, 0.9 g/L), cells (at 80% confluence) were quenched with 600 µL methanol 80% (v/v) on dry ice. The homogenates were then sonicated in ice water slurry for 10 min with the cycling 30s on/off at the highest setting (bath sonicator Biorupter®, Diagenode, NJ, USA) and centrifuged at 14 000 g (4°C) for 10 min. The supernatants, supplemented with internal standard (750 ng myristic acid-D_{27}; Sigma-Aldrich), were dried overnight in cold vacuum centrifuge (Labconco, MO, USA).

GC/MS. The dried samples were dissolved in 30 µL of methoxyamine hydrochloride (10 mg/mL diluted in pyridine; Sigma-Aldrich) with sonication (for 30s) and vortex (for 30s). After incubation for 30 min at room temperature, the samples were derivatized with 70

μL of N-tert-butyldimethylsilyl-N-methyltrifluoroacetamide (MTBSTFA, > 97%; Sigma-Aldrich), transferred in sealed glass vials, and then incubated for 1h at 70°C. GC/MS analysis was performed by injection of 1 μL of derivatized sample into GC/MS instrument (5975C; Agilent, CA, USA). Data acquisition was done in both Scan and SIM (Selected Ion Monitoring) modes as described in (31,32). The isotopic distribution of integrated ions was determined using Agilent MassHunter software. The steady state level was determined for each metabolite and normalized by cell number and internal standard (myristic acid-D_{27}) intensity. Isotopic distributions were corrected for naturally occurring isotopes to isolate contributions from our tracers using an in-house algorithm according to(32,33). Enrichments for specific isotopomers (e.g. m+3), termed proportional ion amount, were presented as proportions of the total isotopic distribution for each metabolite. Total abundance of specific isotopomers, termed relative ion amount, was assessed for each metabolite by multiplying proportional ion amounts by the normalized steady state levels.

NMR Sample preparation. Tumors were flash frozen directly after dissection, ground to a fine powder using a mortar and pestle on liquid nitrogen, weighed (15 to 59 mg) and transferred to 2ml Eppendorf micro-centrifuge tubes. Six pre-washed and chilled 1.4mm ceramic beads were added to each sample along with 1.5 ml of cold 80% methanol in water (both LC/MS grade solvents). The samples were subjected to two minutes of bead beating (TissueLyser II – Qiagen, GmbH, Germany). Precipitated proteins and tissue debris were removed by centrifugation at 15 krpm and 1^{o}C for 10 min. Supernatants were transferred to chilled tubes and dried by vacuum centrifugation (Labconco, Kansas City MO, USA) with sample temperature maintained at -4^{o}C. Samples were subsequently re-

suspended in 230uL water centrifuged at 15 krpm for 10 min at 1^{o}C. A volume of 144 µL of tumour extract along with 16 µL NMR sample buffer were transferred to 3 mm NMR tubes using a Gilson Liquid handler 215 sample preparation robot. The final concentration buffer concentration was 150mM KH_2PO_4, 0.5mM 3-(trimethylsilyl) propionic-2,2,3,3-D_4 acid, 0.2mM NaN_3 at pH 7.4 in 10% D_2O.

NMR Data Collection and Analysis. NMR data were collected at the Drug Discovery Platform (McGill University Health Centre Research Institute) utilizing a Bruker Avance III HD 600MHz NMR spectrometer equipped with a CPQCI ^{1}H-^{31}P/^{13}C/^{15}N cryogenically cooled probe and Sample Jet^{TM} autosampler (Bruker Biospin LTD, Milton, Ontario, Canada). NMR spectra of samples were collected using the first increment of the NOESY pulse sequence supplied with the instrument. Metabolite profiling and quantitation was achieved using Chenomx NMR Suite Professional (v8.2) where 0.5 mM TSP-D_4 was used as the internal concentration standard (https://pubs.acs.org/doi/abs/10.1021/ac060209g). The amount of metabolites was normalized to the weight of the extracted tumor.

Statistical Analysis. Unless otherwise indicated, all *in vitro* studies were carried out with three biological replicates with four technical replicates per experimental group. Data were normalized to the standard curve or the control group as appropriate. For the *in vivo* studies, power analysis showed a sample size of ten tumors per group provided 80% power to detect a mean 1.5-fold difference in tumor volume with a significance level of 0.05 (two-tailed) between two groups. The following statistical analyses were used throughout this study: Two-tailed, paired student's *t* test (Figures 1C, 1D, 2A, 2B, 5A); Two-tailed, unpaired student's *t* test (Figure 1B, 1E-H, 2C-E, 3A, 3B, S6); Two-tailed,

unpaired student's *t* test Holm-Sidak method (Figure 6D-F); One-way ANOVA with a Tukey's multiple comparisons test (Figure 3C-E, 5F-I, S1B-C, S2A); Two-way ANOVA with a Tukey's multiple comparisons test (Figure 4B, 4D, 5B-E, 6C, S2B-D, S5B-C, S7). Statistical significance is shown as follows: *P,0.05; **P<0.01; ***P,0.001, ****P<0.0001.

RESULTS

The ShcA adaptor increases the metabolic rate and glucose dependency of breast tumors. Since the ShcA adaptor is a critical signaling hub downstream of RTKs for mammary tumor initiation, growth and angiogenesis (23,34), we sought to establish whether its also plays a role in metabolic reprogramming. To test this, we modulated ShcA signaling in ErbB2-transformed NMuMG breast cancer cells by ectopically expressing FLAG-tagged ShcA-proficient ($ShcA^{WT}$) or -deficient (Y239/240/313F; Shc3F) alleles. The Shc3F allele serves as a dominant negative mutant (Figure 1A) (25). We show comparable $ShcA^{WT}$-FLAG and Shc3F-FLAG expression levels in both cell lines (Figure S1A). Moreover, expression of the Shc3F mutant severely impairs mammary tumor growth in an orthotopic mouse model relative to $ShcA^{WT}$-controls (Figure 1B). We previously showed that impaired ShcA signaling reduces the proliferative and angiogenic capacities of these tumors *in vivo* (23,24). We now show that Shc3F-expressing cells are less metabolically active, as evidenced by 20% and 10% decreased rates of glycolysis (extracellular acidification rate, ECAR) and mitochondrial respiration (oxygen consumption rate, OCR) compared to $ShcA^{WT}$ cells (Figure 1C). Nonetheless, AMPK Thr-172 phosphorylation was reduced in Shc3F-expressing cells (Figure 1D) and mammary tumors (Figure 1E) compared to their $ShcA^{WT}$ counterparts. This is coincident with reduced AMP levels in Shc3F mammary tumors (Figure 1F). Taken together, these data suggest that RTKs engage the ShcA pathway to promote metabolism.

With the knowledge that many breast tumors acquire a Warburg-like metabolism, we next assessed whether modulating the ShcA pathway in breast cancer cells altered

their glucose dependency. While inhibition of ShcA signaling does not impact breast cancer cell growth in glucose replete conditions (25 mM), Shc3F cells acquire a growth advantage when glucose levels are reduced (5 mM) or absent (0 mM) (Figure 1G). In contrast, ectopic expression of wild-type ShcA sensitizes ErbB2-NMuMG cells to glucose deprivation to levels that are comparable to parental cells (Figure S1B). To further support our findings, we tested the glucose dependency of MT-transformed breast cancer cells that originated from transgenic mice (MT/ShcA$^{+/+}$ vs. MT/ShcA$^{3F/+}$) (25) expressing the Shc3F allele under the control of the endogenous *ShcA* promoter. We show that impaired ShcA signaling increases cell viability upon glucose withdrawal in cells expressing physiological levels of the Shc3F mutant (Figure S1C). These data suggest that reduced ShcA signaling endows breast cancer cells with the potential to grow under glucose-deprived conditions.

We next assessed whether reduced ShcA signaling is associated with impaired glucose metabolism in mammary tumors. We show that inhibition of ShcA signaling (Shc3F) significantly increases glucose levels in mammary tumors relative to ShcA^{WT} controls (Figure 1H). Despite this fact, Shc3F tumors possess reduced lactate levels and a significant reduction in the lactate/glucose ratio compared to ShcA^{WT} tumors (Figure 1H), coincident with their reduced growth potential (Figure 1B). mitochondrial respiration (oxygen consumption rate, OCR) compared to ShcA^{WT} cells (Figure 1C). Moreover, steady state levels of glycolytic and citric acid cycle (CAC) metabolites, including pyruvate, α-ketoglutarate, fumarate and malate were also reduced in Shc3F cells compared to ShcA^{WT} cells (Figure S2A). This suggest that attenuated ShcA

signaling decreases the ability of mammary tumors to metabolize glucose, resulting in a reduced bioenergetic capacity.

To better understand the impact of glucose deprivation on metabolic adaptations in $ShcA^{WT}$ and Shc3F cells, we measured glycolytic and CAC metabolite levels in each cell line cultured in the presence or absence of glucose. Compared to $ShcA^{WT}$ cells, steady state levels of pyruvate along with several CAC metabolites (citrate, α-ketoglutarate, fumarate, malate) are less depleted in Shc3F breast cancer cells upon glucose withdrawal (Figure 2A). This suggests that decreased ShcA signaling reduces the metabolic activity of breast cancers, allowing them to withstand glucose deprivation.

Impaired ShcA signaling increases the glutamine dependency of breast cancer cells.

Given its importance as an alternative energy source in a subset of cancers (8), we investigated whether impaired ShcA signaling instead increases the glutamine dependency of breast cancer cells. We first measured how $ShcA^{WT}$ and Shc3F cancer cells modulate glutamine and glutamate levels following glucose withdrawal. Increased glutamate production may indicate enhanced glutamine metabolism (8). Although glutamine levels are unaffected, Shc3F cells display a robust increase in glutamate levels following glucose deprivation, suggesting that they efficiently metabolize glutamine in the absence of glucose (Figure 2B). We next compared the relative viability of $ShcA^{WT}$ and Shc3F cells in response to glucose versus glutamine deprivation. Whereas Shc3F cells better withstand glucose withdrawal, they are more sensitive to glutamine deprivation relative to $ShcA^{WT}$ controls (Figure 2C). These data suggest that inhibition of ShcA signaling increases the glutamine dependency of breast cancer cells.

Considering these observations, we measured glutamine and glutamate levels in $ShcA^{WT}$ and Shc3F mammary tumors. Compared to $ShcA^{WT}$ controls, tumors with reduced ShcA signaling display increased glutamine levels, coincident with decreased glutamate levels (Figure 2D). The increased lactate/glucose (Figure 1H) and glutamate/glutamine (Figure 2D) ratios in $ShcA^{WT}$-expressing tumors suggests that they increase their bioenergetic capacity through enhanced glucose and glutamine metabolism yet are exquisitely reliant on glucose availability. Even though Shc3F cells reduce their bioenergetic capacity and are less dependent on glucose, they instead reprogram their metabolism to rely on glutamine.

Impaired ShcA signaling sensitizes breast cancers to biguanides.

Biguanides (metformin and phenformin) block complex I of the electron transport chain (12-14) and render cells dependent on glycolysis (10,12,15). We next asked whether inhibition of ShcA signaling in breast cancer cells exposes a metabolic vulnerability to biguanides. In agreement with their reduced glycolytic capacity and enhanced dependence on oxidative phosphorylation, Shc3F cells are more sensitive to phenformin compared to $ShcA^{WT}$ cells *in vitro* (Figure 3A). We next injected $ShcA^{WT}$- and Shc3F-expressing cells into the mammary fat pad of immunodeficient mice to determine whether ShcA signaling impacted the sensitivity of mammary tumors to phenformin *in vivo*. $ShcA^{WT}$ tumor growth is minimally affected by phenformin treatment (Figure 3B), even though we observe increased pAMPK immunohistochemical staining (Figure 3C). Phenformin did not impact the proliferative capacity of $ShcA^{WT}$ tumors (Figure 3D) but increased their apoptotic response (Figure 3E). This is consistent with the inability of

ShcA^{WT} cells to reduce their metabolic rate under nutrient stress (Figure 1G, 2A). The relative insensitivity of ShcA^{WT} tumors to phenformin *in vivo* (Figure 3B) can be explained by their enhanced bioenergetic capacity and metabolic flexibility to increase the rate of glycolysis.

In contrast, the growth potential of Shc3F tumors was significantly blunted (40% reduction in tumor volume) following phenformin treatment *in vivo* (Figure 3B), in agreement with their greater dependency on mitochondrial metabolism. Phenformin increased pAMPK levels in Shc3F tumors and significantly impaired their proliferative capacity but did not alter their apoptotic rate (Figure 3C-E). This suggests that reduced ShcA signaling sensitizes mammary tumors to phenformin through induction of a cytostatic response.

ShcA signaling increases glucose metabolism to confer biguanide resistance. To gain a mechanistic understanding of how ShcA signaling impacts the metabolic network, we performed stable isotope tracing experiments to follow the fate of [U-^{13}C]-glucose in ShcA^{WT} and Shc3F cells (Figure. 4A). These studies allowed us to determine whether ShcA signaling diverts glucose through glycolysis or the citric acid cycle (CAC) for ATP production. ShcA^{WT} and Shc3F cells displayed similar kinetics of [U-^{13}C]-labeling for glycolytic intermediates (Figure 4B). Accounting for the larger steady state pool of each metabolite in ShcA^{WT} cells (Figure 4C, S2B), these data support the fact that ShcA increases the glycolytic capacity of breast cancer cells (Figure 1B), resulting in a higher quantitative glycolytic flux. Despite this fact, the lactate/pyruvate ratio is similar between ShcA^{WT} and Shc3F cells (Figure S2C). These data suggest that ShcA signaling globally

increases glucose metabolism both through glycolysis and conversion to lactate or its metabolism through the CAC. Indeed, we show that the ability of (m+3) pyruvate to enter the CAC, either to generate ATP (green bars) or for macromolecular synthesis (blue bars) is comparable between $ShcA^{WT}$ and Shc3F-expressing cells (Figure 4D, S3). Again, considering the larger pool of CAC metabolites in $ShcA^{WT}$-expressing cells (Figure 4C, S2A), these data reinforce the fact that glucose flow through the CAC is globally increased by elevated ShcA signaling.

As expected, phenformin significantly increased glycolysis in both $ShcA^{WT}$ and Shc3F cells (Figure 4B, S3). Coupled with the drastic increase in the steady state pools of glycolytic metabolites (Figure 4C, S2A), these data are consistent with studies reporting a strict reliance on aerobic glycolysis in the presence of biguanides (10,12,15). While phenformin increased the lactate/pyruvate ratio in $ShcA^{WT}$ and Shc3F-expressing cells, the induction was stronger in $ShcA^{WT}$ cells (Figure S2C). These data indicate that ShcA signaling increases the glycolytic capacity of breast cancer cells, rendering them better able to cope with biguanide treatment (Figure 3A). Moreover, phenformin drastically reduced the forward flow of glucose-derived metabolites into the CAC in both $ShcA^{WT}$ and Shc3F-expressing cells (Figure 4D; Figure S3). In contrast, phenformin promoted anaplerosis (reverse flow) to replenish CAC intermediates. Combined these data suggest that phenformin blocks mitochondrial glucose metabolism independently of the ShcA pathway.

Given that inhibition of ShcA signaling in breast cancer cells increases their glutamine reliance (Figure 2C), we also examined the fate of [U-^{13}C]-glutamine through the CAC. Labelled glutamine (m+5) enters the CAC through the stepwise conversion to

glutamate (m+5) and α-ketoglutarate (m+5). α-ketoglutarate-derived carbons either flow through the canonical CAC (m+4; illustrated in green) or reductive carboxylation (m+5 citrate; m+3 oxaloacetate, m+3 malate; m+3 fumarate; depicted in red) (Figure S4). Reductive carboxylation of glutamine occurs mainly in cancer cells with defective mitochondria or under reductive conditions, like hypoxia and exposure to biguanides (35-37). There was no significant difference in the metabolism of glutamine through the canonical CAC between $ShcA^{WT}$ and Shc3F-expressing cells (Figures S4, S5A, B). Phenformin treatment significantly decreased the flow of glutamine-derived carbons through the canonical CAC in both $ShcA^{WT}$ and Shc3F cells. However, phenformin promoted reductive carboxylation of glutamine in both cell types (Figures S4, S5A, C). These results indicate that perturbation of ShcA signaling does not affect how glutamine is metabolized through the canonical CAC. Although phenformin-treated Shc3F cells displayed an increase in the α-ketoglutarate/citrate ratio (Figure S2D), enhanced reductive carboxylation does not protect them from the anti-tumorigenic effects of this biguanide. Instead, the reduced capacity of Shc3F-expressing cells to engage glycolysis in the presence of phenformin likely explains their increased sensitivity to biguanides, compared to $ShcA^{WT}$ controls.

PGC-1α is essential for ErbB2-driven breast tumor initiation and resistance to biguanides. The PGC-1α transcriptional co-activator is a master regulator of energy metabolism (38) and is induced upon nutrient stress (39). Strikingly, we observed that ShcA signaling increases PGC-1α expression. Indeed, PGC-1α levels are 3.9-fold higher in $ShcA^{WT}$ cells compared to Shc3F cells (Figure 5A). To interrogate whether ShcA

signaling increases the PGC-1α dependency of breast cancer cells, we employed shRNA approaches to stably reduce *Ppargc1a* mRNA levels in cells that differ in their ability to engage the ShcA pathway. This includes ErbB2/ShcA^{WT} and ErbB2/Shc3F cells in addition to two independent explants from MT/ShcA$^{+/+}$ and MT/ShcA$^{+/3F}$ mammary tumors (Figure S6). We show that breast cancer cells with an intact ShcA pathway are more reliant on PGC-1α to support their growth, even under nutrient replete conditions (Figure 5B, C). Moreover, the ability of ShcA signaling to cope with phenformin requires PGC-1α (Figure 5B, C). These data support an essential role for PGC-1α in increasing glucose metabolism (40). Finally, PGC-1α is also required to permit Shc3F cells to withstand glucose withdrawal, further reinforcing its essential role in mitochondrial metabolism (Figure 5B, C).

To further substantiate an essential role for PGC-1α in ShcA-driven breast cancer progression, we ectopically expressed PGC-1α in Shc3F cells or stably deleted *PGC-1α* from ShcA^{WT} and Shc3F cells by Crispr/Cas9 gene editing (Figure 5D, E). We used two independent guides directed to the second exon of *PGC-1α.* PGC-1α null cells encode the first 57 (Crispr #1) or 37 (Crispr #2) amino acids of PGC-1α prior to introduction of a pre-mature stop codon. We show that Shc3F cells better tolerated *PGC-1α* loss, whereas *PGC-1α* was key for ShcA^{WT} cell viability (Figure 5D), confirming the fact that ShcA signaling increases the PGC-1α dependency of breast cancer cells (Figure 5B, C). This suggests that the *PGC-1α*-null, ShcA^{WT} clones likely significantly re-wired their metabolism. Moreover, reduced ShcA signaling permits cancer cells to adapt to PGC-1α

loss under nutrient replete conditions. Hence, we focused our attention on understanding the effects of PGC-1α loss on the tumorigenic potential of Shc3F cells.

We first examined how nutrient deprivation modulated PGC-1α levels in breast cancer cells. Although endogenous *Ppargc1a* (PGC-1α) levels are basally low in Shc3F cells, *Ppargc1a* is strongly induced in these cells (40 fold) upon glucose deprivation. In contrast, PGC-1α overexpressing cells modestly upregulated *Ppargc1a* levels (2 fold) in the absence of glucose (Figure 5E). Moreover, *Ppargc1a* mRNA levels were not appreciably induced in PGC-1α null cells, supporting the fact that PGC-1α transcriptionally controls its own promoter (41) (Figure 5E). We also examined how PGC-1β and ERRα levels are controlled by alterations in ShcA signaling and/or PGC-1α expression. PGC-1β is a closely related family member (42) and ERRα is an orphan nuclear receptor that preferentially dimerizes with PGC-1α to coordinate expression of metabolic genes (43). *Ppargc1b* is modestly repressed in Shc3F cells (1.4 fold), whereas *Esrra* expression is unaffected by the ShcA pathway in high glucose conditions (Figure 5E). Glucose deprivation upregulates *Ppargc1b* and *Esrra* expression in both cell lines. However, Shc3F cells show a greater *Ppargc1b* and *Esrra* induction (Figure 5E). PGC-1α overexpression has little to no impact on endogenous *Ppargc1b* and *Esrra* levels, in glucose-depleted conditions (Figure 5E), given that PGC-1α levels are already significantly induced (Figure. 5A). In contrast, PGC-1α loss significantly impaired the ability of breast cancer cells to upregulate *Ppargc1b* (~2.5 fold) and *Esrra* (~2 fold) following glucose deprivation (Figure 5E).

Next, we tested the impact of PGC-1α overexpression or loss on the growth potential of Shc3F cells. Under control conditions, both PGC-1α overexpression and loss decreased the growth potential of Shc3F cells relative to empty vector controls, suggesting that PGC-1α levels must be tightly controlled to maintain metabolic functions (Figure 5F). Previous studies suggest that cells have a narrow window of tolerance for PGC-1α levels (38,44,45). While PGC-1α overexpression increased the viability of breast cancer cells in response to glucose and glutamine withdrawal, PGC-1α loss further sensitized them to nutrient deprivation (Figure 5G, H). Similarly, PGC-1α overexpression protected breast cancer cells to phenformin while PGC-1α loss further sensitized them to this biguanide (Figure 5I). These data suggest that PGC-1α overexpression endows breast cancer cells with increased metabolic capacities, while PGC-1α loss may be deleterious for cancer cell growth, which requires significant metabolic investment. To test this *in vivo*, we injected $ShcA^{WT}$, Shc3F (EV), PGC-1α overexpressing, PGC-1α Crispr #1 and PGC-1α Crispr #2 cells into the mammary fat pads of immunodeficient mice. As expected, Shc3F cells display delayed tumor onset (Figure 6A) and impaired tumor growth (Figure 6B) relative to $ShcA^{WT}$ cells. PGC-1α overexpression modestly increased tumor onset and growth, suggesting that PGC-1α is insufficient to restore the tumorigenic potential of breast cancers that are debilitated in ShcA signaling. This is consistent with the fact that PGC-1α overexpression did not rescue the proliferative, apoptotic and angiogenic defects of Shc3F tumors (Figure S7).

We also tested whether PGC-1α is necessary for breast cancer progression. Markedly, PGC-1α loss profoundly delayed breast tumor onset (EV: T_{50}=16d; CR1:

T_{50}=48d; CR2: T_{50}=26d) (Figure 6A). As expected, *Sod2* levels (a PGC-1α target gene) were significantly reduced in PGC-1α null cells upon glucose deprivation relative to empty vector controls (Figure 6C). In contrast, *Gls1* levels were comparable between PGC-1α (CR#2) and EV control cells (Figure 6C), which may explain why tumor onset was less severely impaired with the PGC-1α (CR#2) cohort (Figure 6A). However, PGC-1α was dispensable for tumor growth (Figure 6B). This is consistent with the observation that PGC-1α null tumors display comparable rates of proliferation, apoptosis and angiogenesis relative to empty vector controls (Figure S7). Collectively, these data suggest that PGC-1α serves an essential and non-redundant role during tumor emergence. Moreover, significant selective pressures are exerted upon PGC-1α null tumors to re-program their metabolism for subsequent tumor growth. Indeed, we recently showed that PGC-1α increases the global bioenergetic capacity and flexibility of breast cancer cells by increasing ATP production, both through increased glycolysis and oxidative phosphorylation (46).

The ability of biguanides to impair breast tumor initiation is attenuated by deregulated tyrosine kinase signaling. Our results raise the intriguing possibility that metabolic re-programming is a central component of dysregulated tyrosine kinase signaling during the earliest stages of breast cancer progression. To test this, we employed the polyoma virus middle T transgenic mouse model (MMTV/MT). While MT is a viral oncogene and lacks intrinsic kinase activity, it recruits tyrosine kinases and activates many of the same pathways as RTKs (47). We reduced endogenous ShcA signaling using a knock-in allele harbouring phenylalanine substitution of all three tyrosine phosphorylation sites under the

control of the endogenous *ShcA* promoter (MT/ShcA$^{+/3F}$) (29). To inhibit mitochondrial metabolism, MT/ShcA$^{+/+}$ and MT/ShcA$^{+/3F}$ mice were treated with phenformin in the drinking water at first tumor palpation. Compared to the placebo group, phenformin neither impacted the number of tumor bearing glands (Figure 6D) nor the average or total tumor volumes at endpoint in MT/ShcA$^{+/+}$ animals (Figure 6E, F). In stark contrast, phenformin significantly reduced the number of tumor bearing glands (average 8 vs 5 tumors) in MT/ShcA$^{+/3F}$ animals (Figure 6D). Moreover, phenformin-treated MT/ShcA$^{+/3F}$ mice showed a significantly reduced tumor volumes (3.8 fold) compared to control animals (Figure 6E, F). These data suggest that the ability of biguanides to reduce breast cancer incidence critically depends on the ShcA activation status in the breast epithelium.

Taken together, our observations demonstrate that elevated ShcA signaling engages PGC-1α to increase the metabolic rate and bioenergetic flexibility of breast cancers. This ShcA/PGC-1α axis contributes significantly to breast tumor emergence and growth along with resistance to biguanides.

DISCUSSION

Numerous studies have implicated dysregulated receptor tyrosine kinase (RTK) signaling in metabolic re-programming. For example, ErbB2 stimulates glycolytic metabolism in cancer cells, in part, through its ability to upregulate the expression of glycolytic enzymes (20). Breast cancer cells that develop resistance to ErbB2-targeted therapies increase their rate of glycolysis and can also be sensitized to glycolytic inhibitors (5,6). This re-enforces the idea that metabolic reprogramming towards a

glycolytic phenotype is an essential feature of RTK-driven breast tumors. In this study, we provide the first genetic evidence that the ShcA adaptor transduces oncogenic signals that permit metabolic perturbations underlying the glucose dependency of breast cancers.

To cope with their increased metabolic rate, breast tumors that hyperactivate ShcA signaling significantly upregulate PGC-1α levels, leading to elevated mitochondrial metabolism and glucose supply (40). Thus, the ShcA/PGC-1α signaling axis is likely to create a feed forward mechanism to ensure that the proliferative and metabolic needs of aggressive breast tumors are continuously met (Figure 7). This is consistent with the fact that PGC-1α is essential to support a higher metabolic rate in aggressive breast cancers. We recently demonstrated that PGC-1α also promotes bioenergetic flexibility, meaning that elevated PGC-1α levels readily allow cancer cells to switch between mitochondrial and glycolytic metabolism for ATP production (46). Increased ShcA signaling decreases the dependence of breast tumors on either pathway for energy production, rendering them less sensitive to biguanides, which block mitochondrial respiration. In contrast, impaired ShcA signaling lowers PGC-1α levels, which decreases the mitochondrial capacity of breast cancer cells yet renders them more dependent on mitochondrial metabolism, which sensitizes them to biguanides (Figure 7).

Our previous work implicates elevated AKT/mTORC1 signaling as a critical mediator of ShcA-driven breast cancer progression (23). Numerous studies have highlighted an important role for this pathway in cellular metabolism. First, AKT increases glycolytic activity in cancer cells (48). Second, mTORC1 signaling activates a metabolic network, which couples increased glycolysis with protein, nucleotide and lipid synthesis (49). Finally, mTORC1 signaling increases mRNA translation of nuclear-

encoded mitochondrial genes in a 4E-BP dependent manner to augment oxidative phosphorylation (50,51). Our data suggest that ShcA functions as a molecular bridge that allows tyrosine kinases to drive metabolic reprogramming by engaging AKT/mTORC1. Thus, the ShcA pathway may allow breast cancer cells to coordinate signaling (AKT/mTORC1), transcriptional (PGC-1α) and translational (eIF4E) control of tumor metabolism.

Significant research efforts have focused on examining whether biguanides can be re-purposed as anti-cancer agents. Epidemiological and clinical studies have examined whether biguanides associate with decreased risk of developing breast cancer or influence clinical variables associated with tumor growth. For example, a Phase I study where metformin was administered to non-diabetic breast cancer patients in the neo-adjuvant setting showed decreased cell proliferation, which was associated with reduced insulin receptor expression and signaling in metformin-treated tumors (52). This study provided the first experimental evidence that metformin may exert anti-neoplastic activities in breast cancers. Given these observations, activation of the ShcA signaling pathway, may help determine breast cancer patients that would achieve maximal benefit from biguanides.

Globally, our work highlights the importance of metabolism in fuelling RTK/ShcA signalling during all stages of the tumorigenic program. We show that the ShcA pathway increases PGC-1α driven metabolic re-programming to augment the metabolic rate of mammary tumors and render them resistant to agents that target mitochondrial metabolism. This suggests that the ShcA/PGC-1α axis may define sensitivity to

appropriate metabolic-based therapies, both to decrease the risk of disease progression in early stage breast cancer patients and to treat women with invasive carcinoma.

ACKNOWLEDGEMENTS

This work was supported by CIHR grants to JUS (MOP-111143) and JUS and JSP (MOP-244105). We further acknowledge support from the small animal research and pathology core facilities at the Lady Davis Institute and Goodman Cancer Research Centre (GCRC). GC/MS and tracer analyses were performed at the Rosalind and Morris Goodman Cancer Research Centre Metabolomics Core Facility supported by The Dr. John R. and Clara M. Fraser Memorial Trust, the Terry Fox Foundation (TFF Oncometabolism Team Grant 1048 in partnership with the Foundation du Cancer du Sein du Quebec), and McGill University. We are thankful to Dr. Andrée Gravel and Dr. Anne-Laure Larroque for the final NMR sample preparation and data acquisition at the Drug Discovery Platform (MUHC-RI). JUS is the recipient of a Senior FRQS salary support award. JSP and IT acknowledge Junior 2 FRQS salary support awards. YKI, RA and JH were supported by an FRQS Doctoral Award. ON is supported by a Canderel fellowship and SM by a Vanier Canada Graduate Scholarship-CIHR.

REFERENCES

1. Ward PS, Thompson CB. Metabolic reprogramming: a cancer hallmark even warburg did not anticipate. Cancer Cell **2012**;21:297-308
2. Vander Heiden MG, Cantley LC, Thompson CB. Understanding the Warburg effect: the metabolic requirements of cell proliferation. Science **2009**;324:1029-33
3. Groheux D, Cochet A, Humbert O, Alberini JL, Hindie E, Mankoff D. (1)(8)F-FDG PET/CT for Staging and Restaging of Breast Cancer. J Nucl Med **2016**;57 Suppl 1:17S-26S
4. Pelicano H, Martin DS, Xu RH, Huang P. Glycolysis inhibition for anticancer treatment. Oncogene **2006**;25:4633-46
5. Ruprecht B, Zaal EA, Zecha J, Wu W, Berkers CR, Kuster B*, et al.* Lapatinib Resistance in Breast Cancer Cells Is Accompanied by Phosphorylation-Mediated Reprogramming of Glycolysis. Cancer Res **2017**;77:1842-53
6. Zhao Y, Liu H, Liu Z, Ding Y, Ledoux SP, Wilson GL*, et al.* Overcoming trastuzumab resistance in breast cancer by targeting dysregulated glucose metabolism. Cancer Res **2011**;71:4585-97
7. Fendt SM, Bell EL, Keibler MA, Olenchock BA, Mayers JR, Wasylenko TM*, et al.* Reductive glutamine metabolism is a function of the alpha-ketoglutarate to citrate ratio in cells. Nat Commun **2013**;4:2236
8. Hensley CT, Wasti AT, DeBerardinis RJ. Glutamine and cancer: cell biology, physiology, and clinical opportunities. J Clin Invest **2013**;123:3678-84
9. Gross MI, Demo SD, Dennison JB, Chen L, Chernov-Rogan T, Goyal B*, et al.* Antitumor activity of the glutaminase inhibitor CB-839 in triple-negative breast cancer. Mol Cancer Ther **2014**;13:890-901
10. Fendt SM, Bell EL, Keibler MA, Davidson SM, Wirth GJ, Fiske B*, et al.* Metformin decreases glucose oxidation and increases the dependency of prostate cancer cells on reductive glutamine metabolism. Cancer Res **2013**;73:4429-38
11. Foretz M, Guigas B, Bertrand L, Pollak M, Viollet B. Metformin: from mechanisms of action to therapies. Cell Metab **2014**;20:953-66
12. Andrzejewski S, Gravel SP, Pollak M, St-Pierre J. Metformin directly acts on mitochondria to alter cellular bioenergetics. Cancer Metab **2014**;2:12
13. Bridges HR, Jones AJ, Pollak MN, Hirst J. Effects of metformin and other biguanides on oxidative phosphorylation in mitochondria. Biochem J **2014**;462:475-87
14. Wheaton WW, Weinberg SE, Hamanaka RB, Soberanes S, Sullivan LB, Anso E*, et al.* Metformin inhibits mitochondrial complex I of cancer cells to reduce tumorigenesis. Elife **2014**;3:e02242
15. Gravel SP, Hulea L, Toban N, Birman E, Blouin MJ, Zakikhani M*, et al.* Serine deprivation enhances antineoplastic activity of biguanides. Cancer Res **2014**;74:7521-33

16. Cheong JH, Park ES, Liang J, Dennison JB, Tsavachidou D, Nguyen-Charles C*, et al.* Dual inhibition of tumor energy pathway by 2-deoxyglucose and metformin is effective against a broad spectrum of preclinical cancer models. Mol Cancer Ther **2011**;10:2350-62
17. Ogrodzinski MP, Bernard JJ, Lunt SY. Deciphering metabolic rewiring in breast cancer subtypes. Transl Res **2017**;189:105-22
18. Landis J, Shaw LM. Insulin receptor substrate 2-mediated phosphatidylinositol 3-kinase signaling selectively inhibits glycogen synthase kinase 3beta to regulate aerobic glycolysis. J Biol Chem **2014**;289:18603-13
19. Natan S, Tsarfaty G, Horev J, Haklai R, Kloog Y, Tsarfaty I. Interplay Between HGF/SF-Met-Ras Signaling, Tumor Metabolism and Blood Flow as a Potential Target for Breast Cancer Therapy. Oncoscience **2014**;1:30-8
20. Zhao YH, Zhou M, Liu H, Ding Y, Khong HT, Yu D*, et al.* Upregulation of lactate dehydrogenase A by ErbB2 through heat shock factor 1 promotes breast cancer cell glycolysis and growth. Oncogene **2009**;28:3689-701
21. Pelicci G, Lanfrancone L, Grignani F, McGlade J, Cavallo F, Forni G*, et al.* A novel transforming protein (SHC) with an SH2 domain is implicated in mitogenic signal transduction. Cell **1992**;70:93-104
22. Ahn R, Sabourin V, Bolt AM, Hebert S, Totten S, De Jay N*, et al.* The Shc1 adaptor simultaneously balances Stat1 and Stat3 activity to promote breast cancer immune suppression. Nat Commun **2017**;8:14638
23. Im YK, La Selva R, Gandin V, Ha JR, Sabourin V, Sonenberg N*, et al.* The ShcA adaptor activates AKT signaling to potentiate breast tumor angiogenesis by stimulating VEGF mRNA translation in a 4E-BP-dependent manner. Oncogene **2015**;34:1729-35
24. Ursini-Siegel J, Cory S, Zuo D, Hardy WR, Rexhepaj E, Lam S*, et al.* Receptor tyrosine kinase signaling favors a protumorigenic state in breast cancer cells by inhibiting the adaptive immune response. Cancer Res **2010**;70:7776-87
25. Ursini-Siegel J, Hardy WR, Zuo D, Lam SH, Sanguin-Gendreau V, Cardiff RD*, et al.* ShcA signalling is essential for tumour progression in mouse models of human breast cancer. EMBO J **2008**;27:910-20
26. Bergers G, Benjamin LE. Tumorigenesis and the angiogenic switch. Nature reviews Cancer **2003**;3:401-10
27. Ursini-Siegel J, Rajput AB, Lu H, Sanguin-Gendreau V, Zuo D, Papavasiliou V*, et al.* Elevated expression of DecR1 impairs ErbB2/Neu-induced mammary tumor development. Mol Cell Biol **2007**;27:6361-71
28. Guy CT, Cardiff RD, Muller WJ. Induction of mammary tumors by expression of polyomavirus middle T oncogene: a transgenic mouse model for metastatic disease. Mol Cell Biol **1992**;12:954-61
29. Hardy WR, Li L, Wang Z, Sedy J, Fawcett J, Frank E*, et al.* Combinatorial ShcA docking interactions support diversity in tissue morphogenesis. Science **2007**;317:251-6
30. Buescher JM, Antoniewicz MR, Boros LG, Burgess SC, Brunengraber H, Clish CB*, et al.* A roadmap for interpreting (13)C metabolite labeling patterns from cells. Curr Opin Biotechnol **2015**;34:189-201

31. Mamer O, Gravel SP, Choiniere L, Chenard V, St-Pierre J, Avizonis D. The complete targeted profile of the organic acid intermediates of the citric acid cycle using a single stable isotope dilution analysis, sodium borodeuteride reduction and selected ion monitoring GC/MS. Metabolomics **2013**;9:1019-30
32. McGuirk S, Gravel SP, Deblois G, Papadopoli DJ, Faubert B, Wegner A*, et al.* PGC-1alpha supports glutamine metabolism in breast cancer. Cancer Metab **2013**;1:22
33. Nanchen A, Fuhrer T, Sauer U. Determination of metabolic flux ratios from 13C-experiments and gas chromatography-mass spectrometry data: protocol and principles. Methods Mol Biol **2007**;358:177-97
34. Ursini-Siegel J, Muller WJ. The ShcA adaptor protein is a critical regulator of breast cancer progression. Cell Cycle **2008**;7:1936-43
35. Griss T, Vincent EE, Egnatchik R, Chen J, Ma EH, Faubert B*, et al.* Metformin Antagonizes Cancer Cell Proliferation by Suppressing Mitochondrial-Dependent Biosynthesis. PLoS Biol **2015**;13:e1002309
36. Metallo CM, Gameiro PA, Bell EL, Mattaini KR, Yang J, Hiller K*, et al.* Reductive glutamine metabolism by IDH1 mediates lipogenesis under hypoxia. Nature **2011**;481:380-4
37. Mullen AR, Wheaton WW, Jin ES, Chen PH, Sullivan LB, Cheng T*, et al.* Reductive carboxylation supports growth in tumour cells with defective mitochondria. Nature **2011**;481:385-8
38. Austin S, St-Pierre J. PGC1alpha and mitochondrial metabolism--emerging concepts and relevance in ageing and neurodegenerative disorders. J Cell Sci **2012**;125:4963-71
39. Arany Z, Foo SY, Ma Y, Ruas JL, Bommi-Reddy A, Girnun G*, et al.* HIF-independent regulation of VEGF and angiogenesis by the transcriptional coactivator PGC-1alpha. Nature **2008**;451:1008-12
40. Klimcakova E, Chenard V, McGuirk S, Germain D, Avizonis D, Muller WJ*, et al.* PGC-1alpha promotes the growth of ErbB2/Neu-induced mammary tumors by regulating nutrient supply. Cancer Res **2012**;72:1538-46
41. Handschin C, Rhee J, Lin J, Tarr PT, Spiegelman BM. An autoregulatory loop controls peroxisome proliferator-activated receptor gamma coactivator 1alpha expression in muscle. Proc Natl Acad Sci U S A **2003**;100:7111-6
42. Liu C, Lin JD. PGC-1 coactivators in the control of energy metabolism. Acta Biochim Biophys Sin (Shanghai) **2011**;43:248-57
43. Deblois G, St-Pierre J, Giguere V. The PGC-1/ERR signaling axis in cancer. Oncogene **2013**;32:3483-90
44. Ciron C, Lengacher S, Dusonchet J, Aebischer P, Schneider BL. Sustained expression of PGC-1alpha in the rat nigrostriatal system selectively impairs dopaminergic function. Hum Mol Genet **2012**;21:1861-76
45. Shin JH, Ko HS, Kang H, Lee Y, Lee YI, Pletinkova O*, et al.* PARIS (ZNF746) repression of PGC-1alpha contributes to neurodegeneration in Parkinson's disease. Cell **2011**;144:689-702

46. Andrzejewski S, Klimcakova E, Johnson RM, Tabaries S, Annis MG, McGuirk S*, et al.* PGC-1alpha Promotes Breast Cancer Metastasis and Confers Bioenergetic Flexibility against Metabolic Drugs. Cell Metab **2017**
47. Fluck MM, Schaffhausen BS. Lessons in signaling and tumorigenesis from polyomavirus middle T antigen. Microbiol Mol Biol Rev **2009**;73:542-63, Table of Contents
48. Elstrom RL, Bauer DE, Buzzai M, Karnauskas R, Harris MH, Plas DR*, et al.* Akt stimulates aerobic glycolysis in cancer cells. Cancer Res **2004**;64:3892-9
49. Duvel K, Yecies JL, Menon S, Raman P, Lipovsky AI, Souza AL*, et al.* Activation of a metabolic gene regulatory network downstream of mTOR complex 1. Mol Cell **2010**;39:171-83
50. Gandin V, Masvidal L, Hulea L, Gravel SP, Cargnello M, McLaughlan S*, et al.* nanoCAGE reveals 5' UTR features that define specific modes of translation of functionally related MTOR-sensitive mRNAs. Genome Res **2016**;26:636-48
51. Morita M, Gravel SP, Chenard V, Sikstrom K, Zheng L, Alain T*, et al.* mTORC1 controls mitochondrial activity and biogenesis through 4E-BP-dependent translational regulation. Cell Metab **2013**;18:698-711
52. Dowling RJ, Niraula S, Chang MC, Done SJ, Ennis M, McCready DR*, et al.* Changes in insulin receptor signaling underlie neoadjuvant metformin administration in breast cancer: a prospective window of opportunity neoadjuvant study. Breast Cancer Res **2015**;17:32

FIGURE LEGENDS

Figure 1: ***ShcA signaling increases the metabolic activity and glucose dependency of ErbB2-driven breast cancer cells.***

(A) Schematic diagram depicting the ShcA alleles ($ShcA^{WT}$, Shc3F) used in this study. **(B)** $ShcA^{WT}$ and Shc3F tumor growth rate is shown as average tumor volume (mm^3) ± SEM (n=8 tumors each). **(C)** The glycolytic and respiratory activity of $ShcA^{WT}$ and Shc3F cells was assessed by quantifying their extracellular acidification rates (ECAR) and oxygen consumption rates (OCR), respectively (means ± SEM, n=9 per group). **(D)** Immunoblot analysis from $ShcA^{WT}$ and Shc3F cells using pAMPK-, AMPK- and Tubulin-specific antibodies. The data is representative of four independent experiments (± SEM). **(E)** Mammary tumors were subjected to immunohistochemical staining using pAMPK-specific antibodies (% positively stained cells ± SEM (n=8 tumors each)). Representative images are shown (Scale bar = 50 microns). **(F)** AMP levels were quantified in $ShcA^{WT}$ (n=10) and Shc3F (n=11) tumors by NMR analysis (moles AMP/mg tumor tissue ± SEM). **(G)** Cells were cultured under variable glucose concentrations and the number of viable cells was quantified by trypan blue exclusion. The data shows one representative experiment (n=4) ± SD, which was performed in duplicate. **(H)** Glucose and lactate levels were quantified in $ShcA^{WT}$ (n=10) and Shc3F (n=11) mammary tumors by NMR analysis (moles of each metabolite/mg tumor tissue ± SEM). The lactate/glucose ratio was also calculated.

Figure 2: ***Impaired ShcA signaling increases the glutamine dependency of breast cancer cells.*** **(A)** Glycolytic and citric acid cycle (CAC) metabolite levels in $ShcA^{WT}$ and

Shc3F cells cultured in high (25 mM) or no (0 mM) glucose for 3 days. The data is shown as fold change in metabolite levels following glucose withdrawal compared to 25 mM glucose conditions ± SEM and is representative of three independent experiments. Metabolite levels for the high glucose condition (average ± SD) is shown. The raw data can be found in Figure S2A. **(B)** The fold change in steady state glutamine and glutamate levels both under high glucose conditions and 48 hours following glucose withdrawal ± SEM. The data is representative of three independent experiments. **(C)** $ShcA^{WT}$ and Shc3F cells were cultured in the presence or absence of glucose or glutamine for three days. The number of viable cells was quantified by trypan blue exclusion (n=8). The data is representative of two independent experiments and is shown as fold change in viable cells relative to $ShcA^{WT}$ control cells ± SD. **(D)** Glutamine and glutamate levels were quantified in $ShcA^{WT}$ (n=10) and Shc3F (n=11) mammary tumors by NMR analysis (moles of each metabolite/mg tumor tissue ± SEM). The glutamate/glutamine ratio was also calculated.

Figure 3: ***Reduced ShcA signaling sensitizes breast tumors to phenformin.***

(A) $ShcA^{WT}$ and Shc3F cells were cultured in the absence (PBS) or presence of phenformin (0.5 mM) for three days. The percentage of viable cells was quantified by trypan blue exclusion (n=9 each). The data is representative of three independent experiments and is shown as % viable cells relative to $ShcA^{WT}$ control (± SD). **(B)** Mammary fat pad injection of $ShcA^{WT}$ and Shc3F cells into immunodeficient mice. When mammary tumors reached 100-150mm^3, animals were treated daily with phenformin (50 mg/kg intraperitoneally) or PBS as control. Average fold increase in

tumor volume relative to Day 0 of treatment ± SEM (n=10 tumors: PBS control groups; n=12 tumors: phenformin-treated groups). **(C-E)** Mammary tumors were subjected to IHC staining using **(C)** pAMPK, **(D)** Ki67 and **(E)** cleaved Caspase-3 specific antibodies. The data is shown as % positively stained cells ± SEM (n=8 tumors). Lower panel shows representative images (Scale bar = 50 microns).

Figure 4: ***ShcA signaling increases glucose metabolism***. **(A)** Schematic representation of glycolysis and citric acid cycle (CAC), with forward (green, m+2) and reverse (blue, m+3) fluxes, using [U-^{13}C]-glucose, as the metabolite tracer (represented as black, green (m+2) and blue (m+3) dots). Labeled intermediate metabolites were analyzed by GC/MS. The white dots represent the endogenous ^{12}C. **(B)** ShcA^{WT} and Shc3F cells were cultured for 24 hours with 0.5 mM phenformin (Phen) or PBS controls, then incubated with [U-^{13}C]-labelled glucose (25 mM) for 30 seconds to measure incorporation into intracellular glycolytic intermediates. **(C)** Schematic representation of steady state metabolite pools in ShcA^{WT} and Shc3F cells cultured for 24 hours with 0.5 mM phenformin (Phen) or PBS controls (graphed data is shown in Figure S2B). **(D)** Cells were also incubated with [U-^{13}C]-glucose for 15 minutes to label intermediates of CAC. Bar graphs indicate the relative ion amount per cell, expressed as mean metabolite level (± SEM; n=3 for each group) for CAC metabolites (± SEM; n=5 for each group). Green bar: incorporation of glucose into the indicated metabolites by forward flow through the CAC (m+2); blue bar: incorporation of glucose into the indicated metabolites by reverse flow through the CAC (m+3).

Figure 5: ***ShcA signaling renders breast cancer cells dependent on PGC-1α.*** **(A)** Relative *Ppargc1a/Actb* mRNA levels were determined by qRT-PCR analysis. The data is representative of two independent experiments with four replicates per experiment ± SD. **(B)** $ShcA^{WT}$ and Shc3F breast cancer cells were retrovirally infected with PGC-1α shRNAs or empty vector controls and cultured under in the absence of glucose or in the presence of 0.5 mM phenformin for 48 hours. The glutamine deprivation experiments were performed after 24 hours. Cell viability was quantified by trypan blue exclusion. The data is shown as % viable cells relative to nutrient replete conditions (n=4) ± SD for one representative experiment performed in duplicate. **(C)** Two independent MT/$ShcA^{+/+}$ (864, 4788) and MT/$ShcA^{+/3F}$ (6021, 6360) breast cancer cell lines expressing control or PGC-1α shRNAs were tested for their viability as described in panel B. **(D)** The efficiency of generating PGC-1α-null cells using two CRISPR guides is shown. **(E)** The indicated cell lines were cultured in high (25 mM) or no (0 mM) glucose for 24 hours and then subjected to qRT-PCR analysis. The relative *Ppargc1a/Actb. Ppargc1b/Actb* and *Esrra/Actb* ratios were determined. The data is representative of four independent experiments (means ± SEM). *$ShcA^{WT}$ vs Shc3F (EV); $^{\varepsilon}$High vs No Glucose Conditions; $^{\delta}$Shc3F (EV) vs PGC1α-O/E), CR#1) and CR#2. **(F-H)** The indicated cell lines were cultured for three days under **(F)** nutrient replete conditions or in the absence of **(G)** glucose or **(H)** glutamine or in the presence of **(I)** 0.5 mM phenformin. Viable cells were quantified by trypan blue exclusion. The data is shown as # viable cells over three days (n=4) ± SD for one representative experiment performed in duplicate.

Figure 6: ***A functional ShcA/PGC1α signaling axis is required during the earliest stages of breast cancer development.*** **(A)** Mammary fat pad injection of the indicated cells into SCID-Beige mice (n=10 tumors each). Kaplan Meier analysis of the percent tumor free mice over time. **(B)** Average tumor volume (mm^3) ± SEM following first palpation. **(C)** The indicated cell lines were cultured in high (25 mM) or no (0 mM) glucose-containing media for 24 hours and then subjected to qRT-PCR analysis. The relative *SOD2/Actb* and *GLS1/Actb* ratios were determined. The data is representative of four independent experiments (means ± SEM) *$ShcA^{WT}$ vs Shc3F (EV) cells; $^{\varepsilon}$High vs No Glucose Conditions; $^{\delta}$Shc3F (EV) vs PGC1α-O/E, CR#1 or CR#2. **(D-F)** MMTV/$ShcA^{+/+}$ and MMTV/$ShcA^{3F/+}$ transgenic mice were monitored for tumor onset by bi-weekly physical palpation and following detection of one tumor-bearing gland, were either given 200 mg/kg phenformin in their drinking water or received water alone for 4-5 weeks. Tumor bearing days: MT/$ShcA^{+/+}$ (Control) = 39.1 ± 1.6 (n=14); MT/$ShcA^{+/+}$ (Phen) = 39.3 ± 2.5 (n=6); MT/$ShcA^{3F/+}$ (Control) = 44.7 ± 6.2 (n=10); MT/$ShcA^{3F/+}$ (Phen) = 43.6 ± 11.5 (n=5). **(D)** The number of tumor bearing glands at endpoint. The **(E)** average and **(F)** total tumor volumes (mm^3) ± SEM at endpoint.

Figure 7: ***Breast cancer cells engage the ShcA/PGC-1α pathway to increase bioenergetic flexibility and resistance to biguanides.*** Schematic diagram illustrating how tyrosine kinases engage the ShcA pathway to promote metabolic flexibility by increasing PGC-1α expression. This response permits breast cancer cells to efficiently metabolize glucose and glutamine, providing adequate sources of fuel both through aerobic glycolysis and glucose oxidative phosphorylation, rendering them resistant to biguanides.

By decreasing signaling downstream of ShcA, glucose metabolism is debilitated in breast cancer cells, which increases their dependency on mitochondrial metabolism for ATP production, exposing a therapeutic vulnerability to increased biguanide sensitivity.

Figure 1

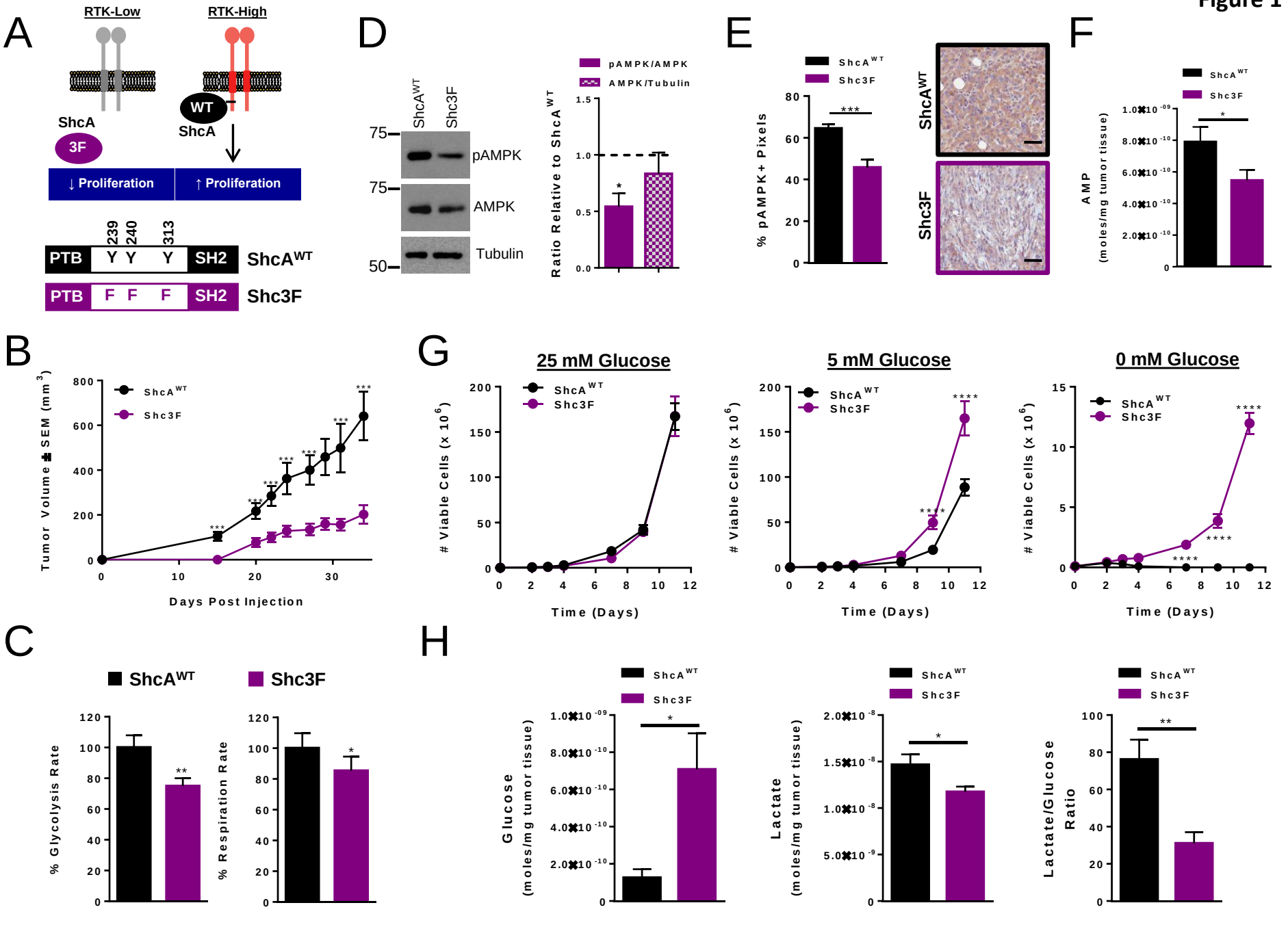
A
RTK-Low
RTK-High
ShcA
3F
WT
ShcA
↓ Proliferation
↑ Proliferation
239 240 313
PTB Y Y Y SH2
ShcA^WT
PTB F F F SH2
Shc3F
B
Tumor Volume ± SEM (mm^3)
ShcA^WT
Shc3F
Days Post Injection
C
ShcA^WT
Shc3F
% Glycolysis Rate
% Respiration Rate
D
ShcA^WT
Shc3F
75
pAMPK
75
AMPK
50
Tubulin
pAMPK/AMPK
AMPK/Tubulin
Ratio Relative to ShcA^WT
E
ShcA^WT
Shc3F
% pAMPK+ Pixels
ShcA^WT
Shc3F
F
ShcA^WT
Shc3F
AMP (moles/mg tumor tissue)
G
25 mM Glucose
5 mM Glucose
0 mM Glucose
ShcA^WT
Shc3F
Viable Cells (x 10^6)
Time (Days)
H
ShcA^WT
Shc3F
Glucose (moles/mg tumor tissue)
Lactate (moles/mg tumor tissue)
Lactate/Glucose Ratio

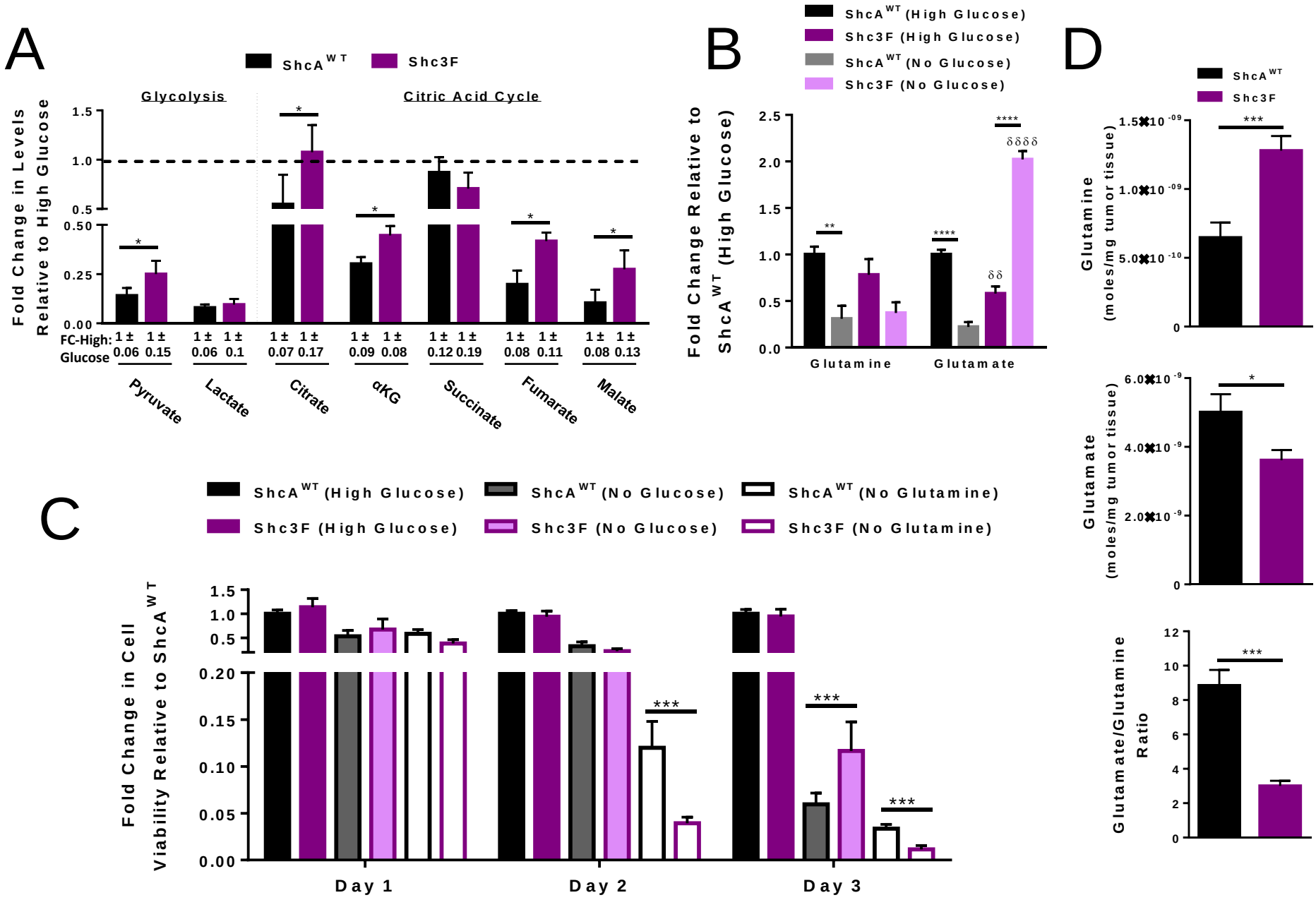
A
ShcA WT
Shc3F
Glycolysis
Citric Acid Cycle
Fold Change in Levels Relative to High Glucose
FC-High Glucose
Pyruvate
Lactate
Citrate
αKG
Succinate
Fumarate
Malate
B
ShcA WT (High Glucose)
Shc3F (High Glucose)
ShcA WT (No Glucose)
Shc3F (No Glucose)
Fold Change Relative to ShcA WT (High Glucose)
Glutamine
Glutamate
C
ShcA WT (High Glucose)
ShcA WT (No Glucose)
ShcA WT (No Glutamine)
Shc3F (High Glucose)
Shc3F (No Glucose)
Shc3F (No Glutamine)
Fold Change in Cell Viability Relative to ShcA WT
Day 1
Day 2
Day 3
D
ShcA WT
Shc3F
Glutamine (moles/mg tumor tissue)
Glutamate (moles/mg tumor tissue)
Glutamate/Glutamine Ratio

Figure 2

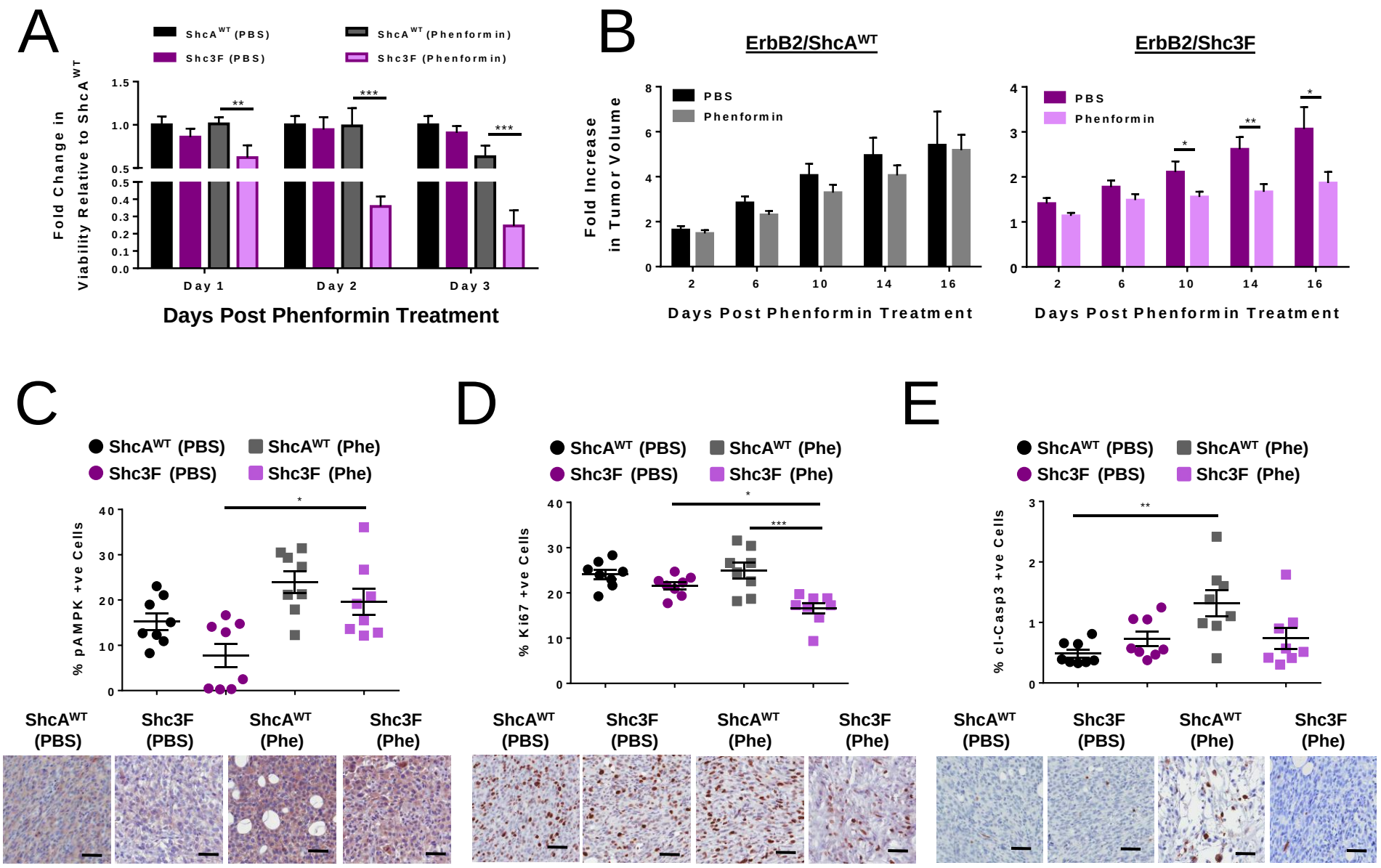
A
ShcA^WT (PBS)
Shc3F (PBS)
ShcA^WT (Phenformin)
Shc3F (Phenformin)
Fold Change in Viability Relative to ShcA^WT
Day 1
Day 2
Day 3
Days Post Phenformin Treatment
B
ErbB2/ShcA^WT
ErbB2/Shc3F
PBS
Phenformin
Fold Increase in Tumor Volume
Days Post Phenformin Treatment
C
ShcA^WT (PBS)
ShcA^WT (Phe)
Shc3F (PBS)
Shc3F (Phe)
% pAMPK +ve Cells
D
% Ki67 +ve Cells
E
% cl-Casp3 +ve Cells

Figure 3

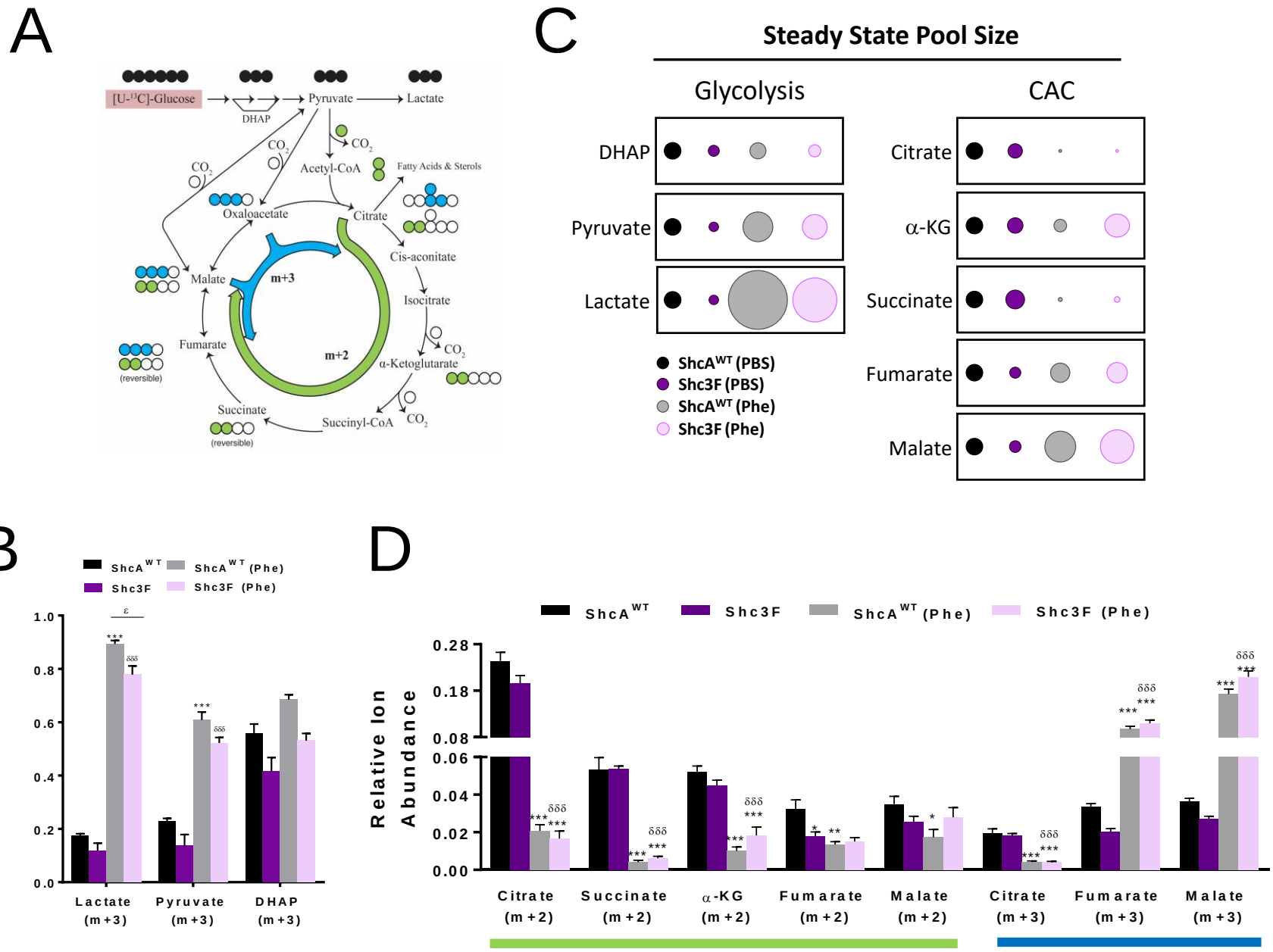
A
[U-13C]-Glucose
DHAP
Pyruvate
Lactate
CO2
Acetyl-CoA
Fatty Acids & Sterols
Oxaloacetate
Citrate
Cis-aconitate
Isocitrate
α-Ketoglutarate
Succinyl-CoA
Succinate
(reversible)
Fumarate
(reversible)
Malate
m+3
m+2
C
Steady State Pool Size
Glycolysis
CAC
DHAP
Pyruvate
Lactate
Citrate
α-KG
Succinate
Fumarate
Malate
ShcA^WT (PBS)
Shc3F (PBS)
ShcA^WT (Phe)
Shc3F (Phe)
B
ShcA^WT
ShcA^WT (Phe)
Shc3F
Shc3F (Phe)
Relative Ion Amount
Lactate (m+3)
Pyruvate (m+3)
DHAP (m+3)
D
Relative Ion Abundance
Citrate (m+2)
Succinate (m+2)
α-KG (m+2)
Fumarate (m+2)
Malate (m+2)
Citrate (m+3)
Fumarate (m+3)
Malate (m+3)

Figure 4

Figure 5

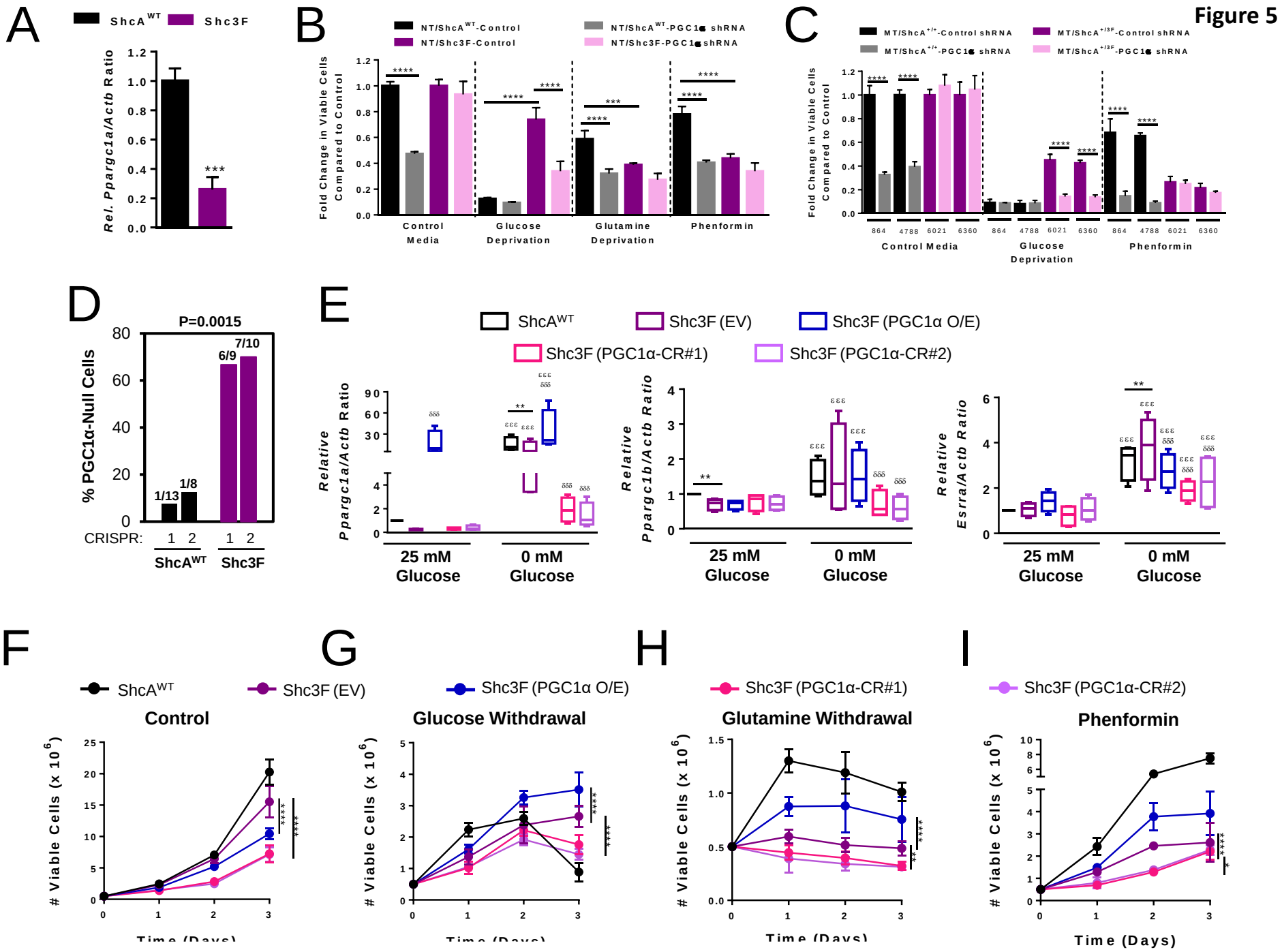
A
ShcA WT
Shc3F
Rel. Ppargc1a/Actb Ratio
***
B
NT/ShcA WT-Control
NT/Shc3F-Control
NT/ShcA WT-PGC1α shRNA
NT/Shc3F-PGC1α shRNA
Fold Change in Viable Cells Compared to Control
Control Media
Glucose Deprivation
Glutamine Deprivation
Phenformin
C
MT/ShcA +/+-Control shRNA
MT/ShcA +/+-PGC1α shRNA
MT/ShcA +/3F-Control shRNA
MT/ShcA +/3F-PGC1α shRNA
Fold Change in Viable Cells Compared to Control
864
4788
6021
6360
Control Media
Glucose Deprivation
Phenformin
D
P=0.0015
% PGC1α-Null Cells
1/13
1/8
6/9
7/10
CRISPR: 1 2 1 2
ShcA WT
Shc3F
E
ShcA WT
Shc3F (EV)
Shc3F (PGC1α O/E)
Shc3F (PGC1α-CR#1)
Shc3F (PGC1α-CR#2)
Relative Ppargc1a/Actb Ratio
Relative Ppargc1b/Actb Ratio
Relative Esrra/Actb Ratio
25 mM Glucose
0 mM Glucose
F
ShcA WT
Shc3F (EV)
Control
Viable Cells (x 10^6)
Time (Days)
G
Shc3F (PGC1α O/E)
Glucose Withdrawal
H
Shc3F (PGC1α-CR#1)
Glutamine Withdrawal
I
Shc3F (PGC1α-CR#2)
Phenformin

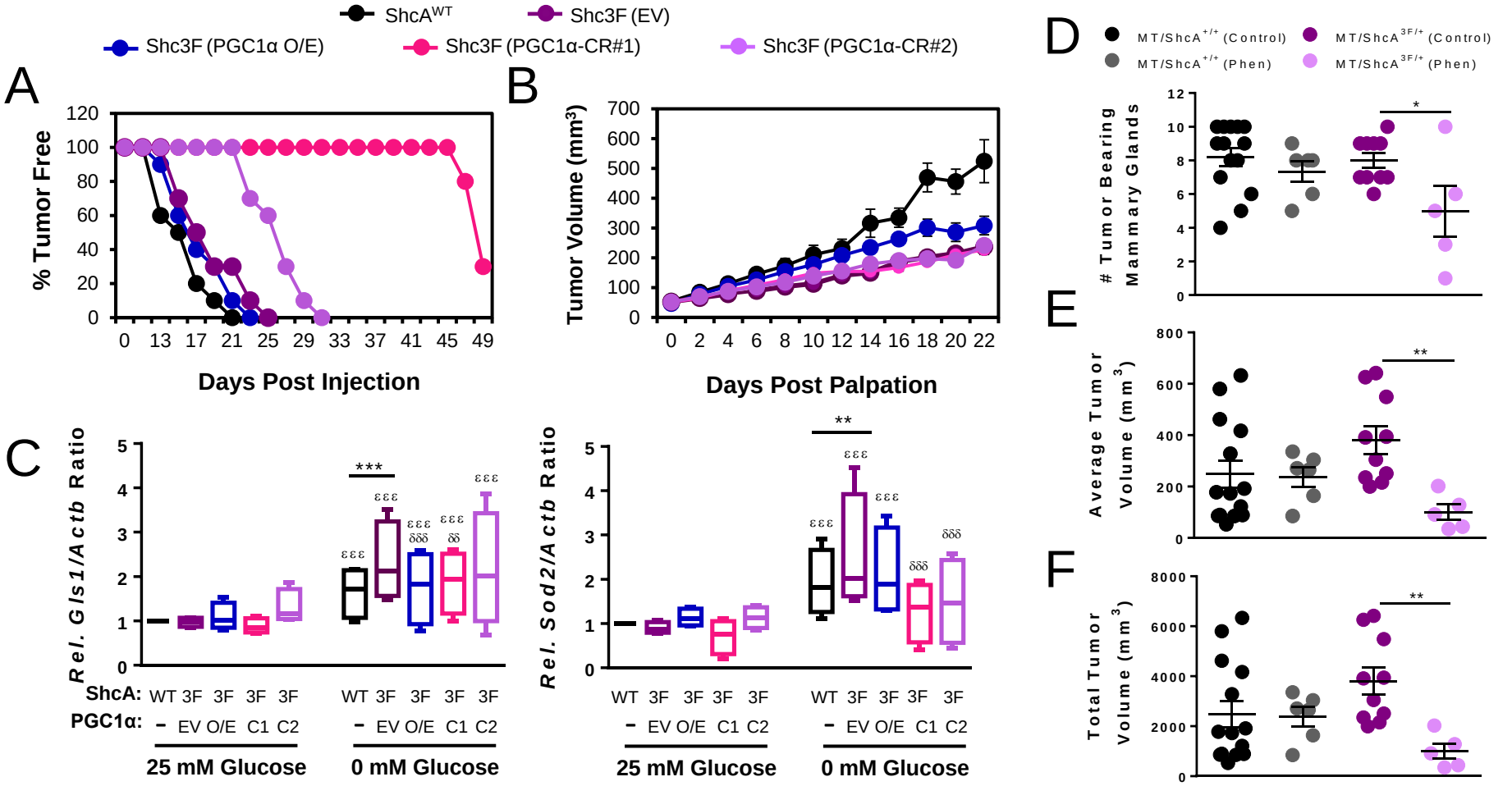
ShcA^WT
Shc3F (EV)
Shc3F (PGC1α O/E)
Shc3F (PGC1α-CR#1)
Shc3F (PGC1α-CR#2)
A
% Tumor Free
Days Post Injection
B
Tumor Volume (mm³)
Days Post Palpation
C
Rel. Gls1/Actb Ratio
Rel. Sod2/Actb Ratio
ShcA: WT 3F 3F 3F 3F WT 3F 3F 3F 3F
PGC1α: – EV O/E C1 C2 – EV O/E C1 C2
25 mM Glucose
0 mM Glucose
D
MT/ShcA+/+ (Control)
MT/ShcA3F/+ (Control)
MT/ShcA+/+ (Phen)
MT/ShcA3F/+ (Phen)
Tumor Bearing Mammary Glands
E
Average Tumor Volume (mm³)
F
Total Tumor Volume (mm³)

Figure 6

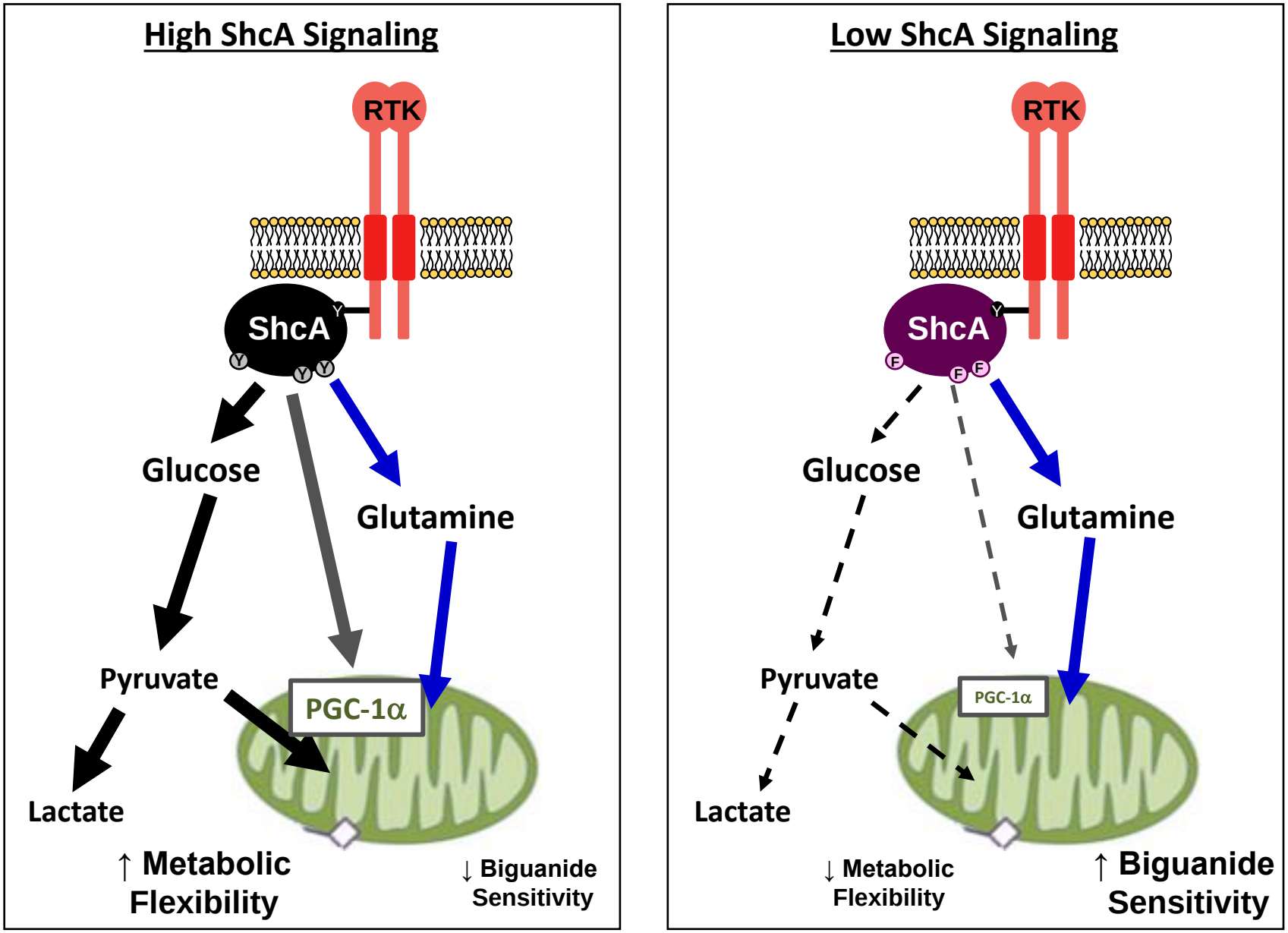
High ShcA Signaling
RTK
ShcA
Y
Y
Y
Y
Glucose
Glutamine
Pyruvate
PGC-1α
Lactate
↑ Metabolic Flexibility
↓ Biguanide Sensitivity
Low ShcA Signaling
RTK
ShcA
Y
F
F
F
Glucose
Glutamine
Pyruvate
PGC-1α
Lactate
↓ Metabolic Flexibility
↑ Biguanide Sensitivity

Figure 7